Dyes and Pigments 81 (2009) 124–130

Contents lists available at ScienceDirect

Dyes and Pigments

journal homepage: www.elsevier.com/locate/dyepig

The synthesis and properties of meso-*tetra*(4-alkylamidophenyl)porphyrin liquid crystals and their Zn complexes

Er-Jun Sun [a,b], Zhao-Yan Sun [c], Mao Yuan [d], Dong Wang [a], Tong-Shun Shi [a,*]

[a] College of Chemistry, Jilin University, Changchun 130023, China
[b] Department of Chemistry, Changchun Normal University, Changchun 130032, China
[c] State Key Laboratory of Polymer Physics and Chemistry, Changchun Institute of Applied Chemistry, Chinese Academy of Sciences, Changchun 130022, China
[d] College of Environment and Resources, Jilin University, Changchun 130023, China

ARTICLE INFO

Article history:
Received 6 August 2007
Received in revised form 25 June 2008
Accepted 26 September 2008
Available online 10 October 2008

Keywords:
Porphyrin
Zn complex
Liquid crystal
Cyclic voltammetry
Surface photovoltage

ABSTRACT

A series of novel, long-chain-substituted, porphyrin derivatives, meso-*tetra* (4-alkylamidophenyl) porphyrin ligands and their Zn complexes (alkyl = 8, 10, 12, 14, 16,18) were prepared by acylation of the amino groups of 5,10,15,20-*tetra*(4-aminophenyl)porphyrin by alkyl chloride. Mesomorphism was investigated by DSC, polarized optical microscopy (POM) and X-ray diffraction (XRD). Only ligands containing chains >12 carbon atoms displayed liquid crystalline behaviour, which exhibited a high phase transition temperature and a broad mesophase temperature span, Zn complexes showed no liquid crystalline behaviour. Cyclic voltammetry, luminescence spectra and surface photovoltage spectroscopy revealed that covalent linking of an alkylamido group to the tetraphenylporphyrin molecule influences, significantly, the properties of the porphyrin macrocycle.

1. Introduction

Porphyrins and metalloporphyrins exist in various states in nature and act as centers of energy transfer and charge transfer processes. In order to reveal their mechanistic role in natural systems, a number of porphyrin derivatives have been synthesized and studied extensively as models of vital functions [1,2]. Moreover, porphyrins are expected to find applications in functional materials because of their favorable electronic properties, chemical and thermal stabilities.

Porphyrin liquid crystals are an important member of the liquid crystal family, which belong to the class of discotic mesogens, as well as triphenylenes [3] and phthalocyanines [4]. The first liquid crystalline porphyrin derivative was reported by Goodby et al. in 1980 [5]. Since then, many mesogenic porphyrins have been synthesized and their mesomorphic properties were investigated [6–13], for example. In 1986, Shimizu et al. found that the 5,10,15,20-tetrakis(4-alkylphenyl)porphyrin derivatives show mesomorphism and they concluded from X-ray studies that the mesophases are discotic lamellar (D_L) phase [6]. In 1989, Bard et al. synthesized octakis(β-hydroxyethy) porphyrin [7]. In 1991 tetrakis(4-*n*-dodecylphenyl) porphyrin was synthesized by Shimizu et al. [8]. In 1998, a new class of meta-substituted bis-pocket porphyrins and metalloporphyrins have been synthesized by Bimal and Kenneth [9]. In 2001, Shi Tongshun and Liu Wei synthesized 5,10,15,20-*tetra* (4-lauroyloxyphenyl)porphyrin and its transition metal complexes which show mesomorphism [10]. But up to now, most of the side chains of TPP derivative liquid crystals are alkyl, alkoxy, or acyloxy group, those containing the alkylamido group as side chains porphyrin liquid crystals have been reported only a little [11]. In this paper, we synthesized a series of 5,10,15,20-*tetra*-(4-alkylamidophenyl)porphyrin ligands and their Zn complexes (shown in Scheme 1) and studied their mesomorphism properties. Results show that only the ligands with long chains of more than 12 carbon atoms have liquid crystalline behaviour, while the Zn complexes are not liquid crystals.

The discotic mesophases have been utilized in (semi)conducting [14] and photoconducting [15] devices, light-emitting diodes [16] and sensors [17]. Other applications of discotic mesogens include their use as optical layers in liquid crystal displays (LCDs), as optical data storage media [18] and as ferroelectric switchable liquid crystals in LCDs [19]. So it is useful to study the properties of porphyrin liquid crystals. In this paper, we investigated these compounds by cyclic voltammetry, surface photovoltage and luminescence spectroscopy, and these studies will provide wider ground for choice and application of the materials.

* Corresponding author. Tel./fax: +86 431 85168898.
E-mail address: sunerjun1974@hotmail.com (T.-S. Shi).

0143-7208/$ – see front matter © 2008 Elsevier Ltd. All rights reserved.
doi:10.1016/j.dyepig.2008.09.016

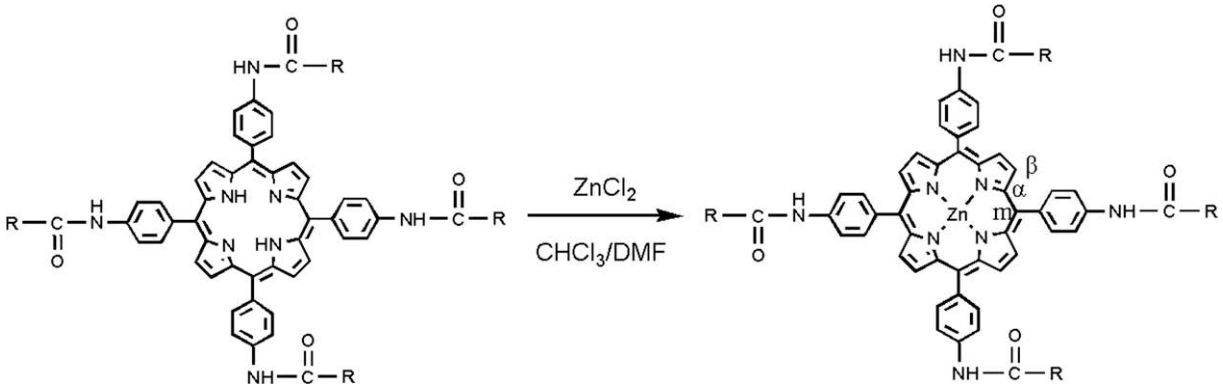

Scheme 1. The structures of porphyrin ligands and Zn complexes. R = C_nH_{2n+1}, (a) Ligands: n = 7, 9, 11, 13, 15, 17 correspond to **8L**, **10L**, **12L**, **14L**, **16L** and **18L**, respectively; (b) Zn complexes: n = 7, 9, 11, 13, 15, 17 correspond to **8Zn**, **10Zn**, **12Zn**, **14Zn**, **16Zn** and **18Zn**, respectively.

2. Experimental

2.1. Materials and physical measurements

All reagents and solvents were of the commercial reagent grade and were used without further purification except DMF was predried over activated 4-Å molecular sieve and vacuum distilled from calcium hydride (CaH_2) prior to use. The dry CH_3CN was obtained by redistillation from CaH_2.

^{1}H NMR spectra were recorded on a Varian–Unity–500(MHz) NMR spectrometer. Chemical shifts were reported on d-scale relative to tetramethylsilane (TMS). Elemental analyses were measured by a Perkin–Elmer 240C auto elementary analyzer. UV–vis spectra were collected on a Shimadzu UV-240 spectrometer. Infrared spectra were recorded on a Nicolet 5PC-FT-IR spectrometer in the region 4000–400 cm^{-1}. Redox potentials of the compounds (10^{-3} mol/L) in dried DMF containing 0.1 mol/L TBAP as a supporting electrolyte were determined at room temperature by cyclic voltammetry with a CHI 660A electrochemical analyzer using a three-electrode system under deaerated conditions. Platinum disk and platinum wire were used as working and counter electrodes. The reversibility of the electrochemical processes was evaluated by standard procedures, and all potentials were recorded against an Ag/Ag^+ reference electrode (0.01 mol/L $AgNO_3$ in acetonitrile solution). Fluorescence spectra were recorded with an SPEX Fluorolog-2T2 spectrofluorometer (450-W xenon lamp as the excitation source). Surface photovoltage spectroscopies were measured with a solid junction photovoltaic cell (ITO/sample/ITO) using light source-monochromator-lock-in detection technique. The differential scanning calorimetry (DSC) was performed with a Perkin–Elmer 7 series thermal analysis system at a scan rate of 10 °C/min under nitrogen flow. X-ray diffraction (XRD) measurements were obtained using a Rigaku X-ray diffractometer with Cu Kα radiation.

2.2. Synthesis of ***10L***

10L was prepared by the reaction of the 5,10,15,20-*tetra* (4-aminophenyl)porphyrin ($TAPPH_2$) which was synthesized in our laboratory according to the method of Kruper [20] with decanoyl chloride. $TAPPH_2$ (1.00 g) was dissolved in freshly distilled $CHCl_3$ (150 ml), and triethylamine (2 ml) was added. A solution of decanoyl chloride (2.8 ml) in $CHCl_3$ (10 ml) was added drop wise to the above solution within 2 h with stirring at 70 °C. The reaction solution then was refluxed for 8 h and cooled to room temperature. Then 200 ml distilled water was added to the reaction mixture and extracted three times by equal volumes of freshly distilled chloroform. The chloroform solution was concentrated and applied to a silica gel column, and the column was eluted with $CHCl_3$–C_2H_5OH (9:1, V/V). The first band was collected and condensed. The precipitated product was crystallized from chloroform and ethanol and was obtained as purple solid. Yield: 38.5%. ^{1}H NMR δ_H (DMSO-d_6, 500 Hz): 10.324 (s, 4H, –NH–CO–), 8.869 (s, 8H, pyrrole ring), 8.124–8.144 (d, 8H, o-C_6H_4), 8.049–8.068 (d, 8H, m-C_6H_4), 1.715–1.740 (t, 8H, –CO–CH_2–), 1.227–1.405 (m, 56H, alkyl CH_2), 0.877–0.891 (t, 12H, alkyl CH_3), −2.886 (s, 2H, pyrrole N–H). Elemental analysis: Calcd for $C_{84}H_{106}N_8O_4$: C 78.09, H 8.27, N 8.68; Found: C 78.18, H 8.22, N 8.70. IR (KBr, υ cm^{-1}): 3315 (ν N–H (pyrrole)), 2924, 2852 (ν C–H), 1664 (ν C═O), 1521 (δ N–H (amide)), 966 (δ N–H (pyrrole)). UV–vis (DMF) λ/nm: 425, 520, 555, 595 and 650 nm.

2.3. Synthesis of ***10Zn***

The complex **10Zn** was prepared by the reaction of **10L** (0.20 g) with $ZnCl_2$ (2.00 g) in $CHCl_3$ (20 ml) and DMF (20 ml) mixture at 70 °C under the protection of nitrogen stream for about 3 h. The extent of the reaction was monitored by measuring the UV–vis spectrum of the reaction solution. The reaction mixture then was chromatographed on silica gel column (eluent:$CHCl_3$–C_2H_5OH 9:1) and crystallized from chloroform and ethanol. Yield: 87.5%. ^{1}H NMR δ_H (DMSO-d_6, 500 Hz): 10.279 (s, 4H, –NH–CO–), 8.808 (s, 8H, pyrrole ring), 8.066–8.083 (d, 8H, o-C_6H_4), 8.012–8.031 (d, 8H, p-C_6H_4), 1.711–1.749 (t, 8H, –CO–CH_2–), 1.283–1.425 (m, 56H, alkyl CH_2), 0.844–0.875 (t, 12H, alkyl CH_3). Elemental analysis: Calcd for $C_{84}H_{104}N_8O_4Zn$: C 74.44, H 7.74, N 8.27; Found: C 74.52, H 7.80, N 8.22. IR (KBr, υ cm^{-1}): 3300 (ν N–H (amide)), 2924, 2852 (ν C–H), 1661 (ν C═O), 1527 (δ N–H (amide)). UV–vis (DMF) λ/nm: 430, 560 and 605 nm.

The preparation methods and results of other ligands and Zn complexes are similar to those mentioned above.

2.3.1. Compound ***8L***

^{1}H NMR δ_H (DMSO-d_6, 500 Hz): 10.315 (s, 4H, –NH–CO–), 8.870 (s, 8H, pyrrole ring), 8.125–8.148 (d, 8H, o-C_6H_4), 8.054–8.070 (d, 8H, m-C_6H_4), 1.733–1.748 (t, 8H, –CO–CH_2–), 1.221–1.410 (m, 56H, alkyl CH_2), 0.845–0.865 (t, 12H, alkyl CH_3), −2.889 (s, 2H, pyrrole N–H). Elemental analysis: Calcd for $C_{76}H_{90}N_8O_4$: C 77.38, H 7.69, N 9.50; Found: C 77.45, H 7.74, N 9.46. IR (KBr, υ cm^{-1}): 3315 (ν N–H (pyrrole)), 2926, 2854 (ν C–H), 1666 (ν C═O), 1520 (δ N–H (amide)), 966 (δ N–H (pyrrole)). UV–vis (DMF) λ/nm: 425, 520, 555, 595 and 650 nm.

2.3.2. Compound ***12L***

^{1}H NMR δ_H (DMSO-d_6, 500 Hz): 10.304 (s, 4H, –NH–CO–), 8.863 (s, 8H, pyrrole ring), 8.122–8.141 (d, 8H, o-C_6H_4), 8.051–8.069

(d, 8H, m-C_6H_4), 1.699–1.756 (t, 8H, –CO–CH_2–), 1.283–1.420 (m, 72H, alkyl CH_2), 0.855–0.882 (t, 12H, alkyl CH_3), −2.894 (s, 2H, pyrrole N–H). Elemental analysis: Calcd for $C_{92}H_{122}N_8O_4$: C 78.70, H 8.76, N 7.98; Found: C 78.61, H 8.68, N 7.88. IR (KBr, υ cm^{-1}): 3313 (ν N–H (pyrrole)), 2924, 2852 (ν C–H), 1662 (ν C═O), 1529 (δ N–H (amide)), 968 (δ N–H (pyrrole)). UV–vis (DMF) λ/nm: 425, 520, 555, 595 and 650 nm.

2.3.3. Compound **14L**

^{1}H NMR δ_H (DMSO-d_6, 500 Hz): 10.308 (s, 4H, –NH–CO–), 8.865 (s, 8H, pyrrole ring), 8.120–8.137 (d, 8H, o-C_6H_4), 8.050–8.067 (d, 8H, m-C_6H_4), 1.713–1.742 (t, 8H, –CO–CH_2–), 1.271–1.419 (m, 88H, alkyl CH_2), 0.829–0.856 (t, 12H, alkyl CH_3), −2.898 (s, 2H, pyrrole N–H). Elemental analysis: Calcd for $C_{100}H_{138}N_8O_4$: C 79.21, H 9.17, N 7.39; Found: C 79.29, H 9.11, N 7.34. IR (KBr, υ cm^{-1}): 3310 (ν N–H (pyrrole)), 2924, 2852 (ν C–H), 1661 (ν C═O), 1524 (δ N–H (amide)), 968 (δ N–H (pyrrole)). UV–vis (DMF) λ/nm: 425, 520, 555, 595 and 650 nm.

2.3.4. Compound **16L**

^{1}H NMR δ_H (DMSO-d_6, 500 Hz): 10.331 (s, 4H, –NH–CO–), 8.859 (s, 8H, pyrrole ring), 8.118–8.133 (d, 8H, o-C_6H_4), 8.046–8.063 (d, 8H, m-C_6H_4), 1.703–1.738 (t, 8H, –CO–CH_2–), 1.267–1.423 (m, 88H, alkyl CH_2), 0.821–0.865 (t, 12H, alkyl CH_3), −2.908 (s, 2H, pyrrole N–H). Elemental analysis: Calcd for $C_{108}H_{154}N_8O_4$: C 79.66, H 9.53, N 6.88; Found: C 79.72, H 9.58, N 6.93. IR (KBr, υ cm^{-1}): 3315 (ν N–H (pyrrole)), 2924, 2852 (ν C–H), 1661 (ν C═O), 1526 (δ N–H (amide)), 966 (δ N–H (pyrrole)). UV–vis (DMF) λ/nm: 425, 520, 555, 595 and 650 nm.

2.3.5. Compound **18L**

^{1}H NMR δ_H (DMSO-d_6, 500 Hz): 10.318 (s, 4H, –NH–CO–), 8.857 (s, 8H, pyrrole ring), 8.121–8.130 (d, 8H, o-C_6H_4), 8.055–8.067 (d, 8H, m-C_6H_4), 1.712–1.742 (t, 8H, –CO–CH_2–), 1.258–1.425 (m, 88H, alkyl CH_2), 0.818–0.859 (t, 12H, alkyl CH_3), −2.890 (s, 2H, pyrrole N–H). Elemental analysis: Calcd for $C_{116}H_{170}N_8O_4$: C 80.04, H 9.84, N 6.44; Found: C 80.13, H 9.78, N 6.47. IR (KBr, υ cm^{-1}): 3318 (ν N–H (pyrrole)), 2922, 2852 (ν C–H), 1661 (ν C═O), 1526 (δ N–H (amide)), 968 (δ N–H (pyrrole)). UV–vis (DMF) λ/nm: 425, 520, 555, 595 and 650 nm.

2.3.6. Compound **8Zn**

^{1}H NMR δ_H (DMSO-d_6, 500 Hz): 10.284 (s, 4H, –NH–CO–), 8.804 (s, 8H, pyrrole ring), 8.078–8.092 (d, 8H, o-C_6H_4), 8.004–8.022 (d, 8H, p-C_6H_4), 1.703–1.746 (8H, –CO–CH_2–), 1.169–1.400 (m, 72H, alkyl CH_2), 0.883–0.918 (t, 12H, alkyl CH_3). Elemental analysis: Calcd for $C_{76}H_{88}N_8O_4Zn$: C 73.44, H 7.14, N 9.02; Found: C 73.53, H 7.09, N 8.94. IR (KBr, υ cm^{-1}): 2924, 2852 (ν C–H), 1662 (ν C═O), 1526 (δ N–H (amide)). UV–vis (DMF) λ/nm: 430, 560 and 605 nm.

2.3.7. Compound **12Zn**

^{1}H NMR δ_H (DMSO-d_6, 500 Hz): 10.261 (s, 4H, –NH–CO–), 8.801 (s, 8H, pyrrole ring), 8.072–8.088 (d, 8H, o-C_6H_4), 8.010–8.027 (d, 8H, p-C_6H_4), 1.700–1.745 (8H, –CO–CH_2–), 1.279–1.407 (m, 72H, alkyl CH_2), 0.858–0.885 (t, 12H, alkyl CH_3). Elemental analysis: Calcd for $C_{92}H_{120}N_8O_4Zn$: C 75.30, H 8.24, N 7.64; Found: C 75.42, H 8.31, N 7.70. IR (KBr, υ cm^{-1}): 2924, 2852 (ν C–H), 1662 (ν C═O), 1526 (δ N–H (amide)). UV–vis (DMF) λ/nm: 430, 560 and 605 nm.

2.3.8. Compound **14Zn**

^{1}H NMR δ_H (DMSO-d_6, 500 Hz): 10.275 (s, 4H, –NH–CO–), 8.800 (s, 8H, pyrrole ring), 8.071–8.087 (d, 8H, o-C_6H_4), 8.010–8.028 (d, 8H, p-C_6H_4), 1.713–1.741 (t, 8H, –CO–CH_2–), 1.275–1.419 (m, 88H, alkyl CH_2), 0.838–0.865 (t, 12H, alkyl CH_3). Elemental analysis: Calcd for $C_{100}H_{136}N_8O_4Zn$: C 76.04, H 8.68, N 7.09; Found: C 75.98, H 8.61, N 7.03. IR (KBr, υ cm^{-1}): 2924, 2852 (ν C–H), 1661 (ν C═O), 1527 (δ N–H (amide)). UV–vis (DMF) λ/nm: 430, 560 and 605 nm.

2.3.9. Compound **16Zn**

^{1}H NMR δ_H (DMSO-d_6, 500 Hz): 10.283 (s, 4H, –NH–CO–), 8.804 (s, 8H, pyrrole ring), 8.065–8.082 (d, 8H, o-C_6H_4), 8.008–8.023 (d, 8H, p-C_6H_4), 1.706–1.745 (t, 8H, –CO–CH_2–), 1.263–1.415 (m, 88H, alkyl CH_2), 0.827–0.860 (t, 12H, alkyl CH_3). Elemental analysis: Calcd for $C_{108}H_{152}N_8O_4Zn$: C 76.67, H 9.06, N 6.62; Found: C 76.81, H 9.14, N 6.55. IR (KBr, υ cm^{-1}): 2924, 2852 (ν C–H), 1661 (ν C═O), 1527 (δ N–H (amide)). UV–vis (DMF) λ/nm: 430, 560 and 605 nm.

2.3.10. Compound **18Zn**

^{1}H NMR δ_H (DMSO-d_6, 500 Hz): 10.286 (s, 4H, –NH–CO–), 8.806 (s, 8H, pyrrole ring), 8.074–8.090 (d, 8H, o-C_6H_4), 8.013–8.032 (d, 8H, p-C_6H_4), 1.716–1.749 (t, 8H, –CO–CH_2–), 1.270–1.425 (m, 88H, alkyl CH_2), 0.830–0.876 (t, 12H, alkyl CH_3). Elemental analysis: Calcd for $C_{116}H_{168}N_8O_4Zn$: C 77.23, H 9.39, N 6.21; Found: C 77.34, H 9.32, N 6.29. IR (KBr, υ cm^{-1}): 2924, 2852 (ν C–H), 1661 (ν C═O), 1527 (δ N–H (amide)). UV–vis (DMF) λ/nm: 430, 560 and 605 nm.

3. Results and discussion

3.1. Liquid crystalline behaviour

The crystalline phase is characterized by DSC, POM and XRD. Only the porphyrin ligands of **12L**, **14L**, **16L** and **18L** are liquid crystals while **8L**, **10L** and all the Zn complexes are not. The calorimetric data of porphyrin liquid crystals are listed in Table 1. All phase transitions are enantiotropic. Each of the ligands exhibits one or two mesophases. It shows a high transition temperature and a broad mesophase temperature span. The lowest temperature for the transition from crystal to liquid-crystal phase is 115 °C (**18L**) and the highest is 182 °C (**12L**). The broadest mesophase temperature span is 160 °C (**16L** and **18L**) and the narrowest is 78 °C (**12L**). With increasing the length of the side chains, the mesophase temperature span increased and the transition temperature decreased.

According to the DSC thermogram of the **14L** (shown in Fig. 1), the ligand melted at 163 °C and discotic mesophase (D_1) was obtained. When heated to 177 °C, another mesophase (D_2) was obtained and it persisted until about 274 °C. On cooling from the isotropic liquid, **14L** changed to first mesophase D_2 at 246 °C, which persisted until near 173 °C and D_1 was obtained. When cooled to 155 °C, the liquid crystal phase changed to crystal phase. The phases are identified by their characteristic optical texture as shown in Fig. 2.

The wide-angle XRD (WAXD) patterns of **18L** at 150 °C in the liquid crystalline phase is shown in Fig. 3. The X-ray diffraction pattern for this compound gives three narrow peaks in the low angle region at 26.0, 12.5 and 9.1 Å, which are in a ration of 1:1/2:1/3, which is evidence of a lamellar structure [21].

The Zn complexes showed no liquid crystal behaviour. As we know, most discotic liquid crystals have a molecular structure that

Table 1
Calorimetric data for compounds **12L**, **14L**, **16L** and **18L**.

Compound		T/°C (ΔH/kJ·mol^{-1})[a]	ΔT/°C[b]
12L	Heating	C[c] 182 (10.52) D[d] 270 (41.96) I[e]	88
	Cooling	I 252 (−50.52) D 174 (−13.53) C	78
14L	Heating	C 163 (25.36) D_1 177 (10.80) D_2 274 (57.31) I	111
	Cooling	I 246 (−54.47) D_2 173 (−23.72) D_1 155 (−15.64) C	91
16L	Heating	C 121 (3.66) D_1 156 (77.59) D_2 281 (77.36) I	160
	Cooling	I 265 (−46.14) D_2 148 (−43.71) D_1 112 (−3.64) C	153
18L	Heating	C 115 (4.20) D_1 143 (67.91) D_2 275 (57.09) I	160
	Cooling	I 251 (−53.99) D_2 131 (−57.94) D_1 106 (−4.44) C	145

[a] Heating rate 10 °C/min, cooling rate 10 °C/min.
[b] Temperature range of liquid crystal.
[c] Crystal.
[d] Discotic mesophase.
[e] Isotropic liquid.

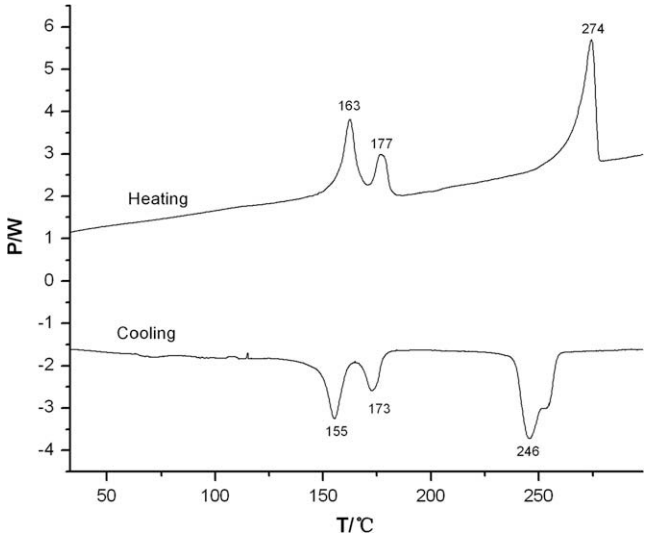

Fig. 1. DSC thermogram of **14L** for heating and cooling rates at 10 °C/min.

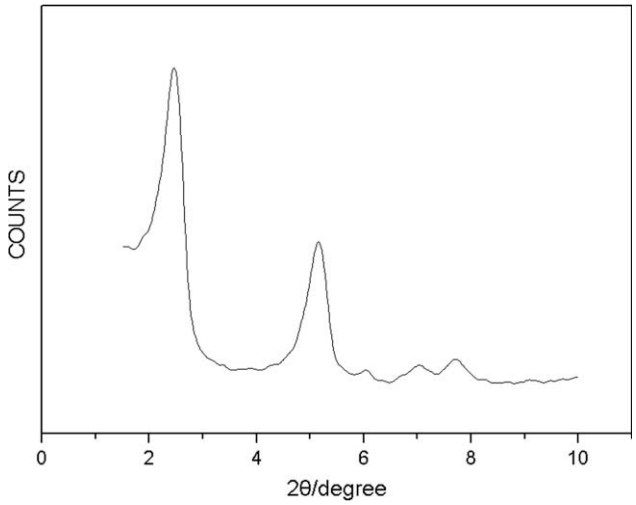

Fig. 3. X-ray diffraction pattern of **18L** at 150 °C.

consists of a flat central core with several flexible chains placed around the outside edge of the core. But there is non-coplanarity of Zn complexes and this structure is unfavorable for the whole macromolecule to pack closely to form discotic liquid crystal. On the other hand, the self-assembly of the metal porphyrins may be another reason. The amide N of the side chains may coordinate to the metal ion of the metal porphyrin which forms complicated multiporphyrin aggregation.

3.2. UV–vis and luminescence spectra

The UV–vis absorption bands of the porphyrins are due to the electronic transitions from the ground state (S_0) to the two lowest singlet excited states S_1 (Q state) and S_2 (Soret state) [22]. The $S_0 \rightarrow S_1$ transition gives rise to the weak Q bands in visible region while $S_0 \rightarrow S_2$ transition produces the strong Soret band in near-UV region. Fig. 4 displays the absorption spectra of TPP, **10L** and **10Zn**. The absorption bands of the free base **10L** appear at 425, 520, 555, 595 and 650 nm. The Soret band is shifted to the red region by 10 nm compared to the TPP spectrum. The Q band consist of four absorption peaks which are typical of $Q_x(0,0)$, $Q_x(0,1)$, $Q_y(0,0)$, $Q_y(0,1)$ transitions in the free base porphyrin. It is seen that the absorption spectrum of **10L** in this region differs from that of TPP: the positions of absorption band maxima are shifted to the red region by 5–10 nm, and the relative intensities of bands I–IV of TPP and **10L** are different. This indicates that covalent linking of alkylamido group to the TPP molecule significantly changes the self-conjugated π-electron system of the porphyrin molecule. The absorption bands of the **10Zn** appear at 430, 560, 605 nm and the spectral patterns are similar to those of the five-coordinated zinc porphyrins, because the amide N may coordinate to the Zn. The decrease in the number of Q bands and the shift in absorption frequencies observed for complexes, relative to the porphyrin ligands, are the result of the increased molecular symmetry of metal complexes [23]. The spectra of other ligands and Zn complexes are similar to **10L** and **10Zn**.

Fig. 5 shows the emission spectra of TPP, **10L** and **10Zn** in DMF (excitation wavelength is 420 nm) and the emission spectral data are given in Table 2. There are fluorescence of the S_2 (Soret band) and the S_1 (Q band) in porphyrin complexes. The fluorescence of $S_2 \rightarrow S_0$ is too weak to be observed in this work. Fluorescence spectra of TPP and **10L** are similar in shape, and they consist of two bands $Q_x(0,0)$ and $Q_x(1,0)$ which are mirror symmetric to the absorption bands I and II. The $Q_x(0,0)$ and $Q_x(1,0)$ fluorescent bands of porphyrin ligands are in the regions of 655–657 and 717–720 nm, respectively. Compared with the fluorescent bands at 653 and 715 nm of TPP, the emission peaks of porphyrin ligands have shifted

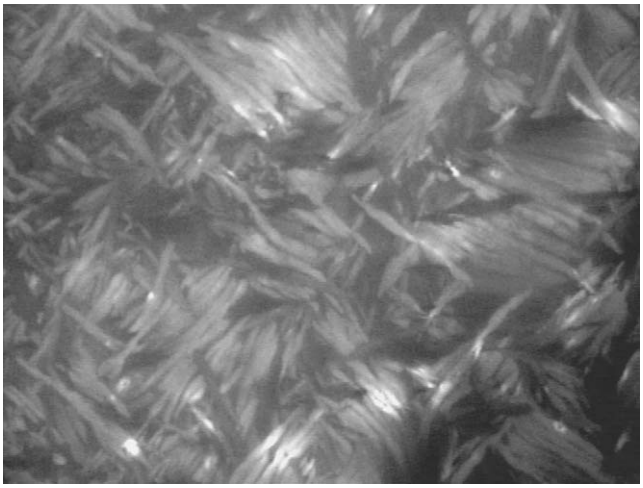

Fig. 2. POM texture of **14L**, cooling from the isotropic state, ×200.

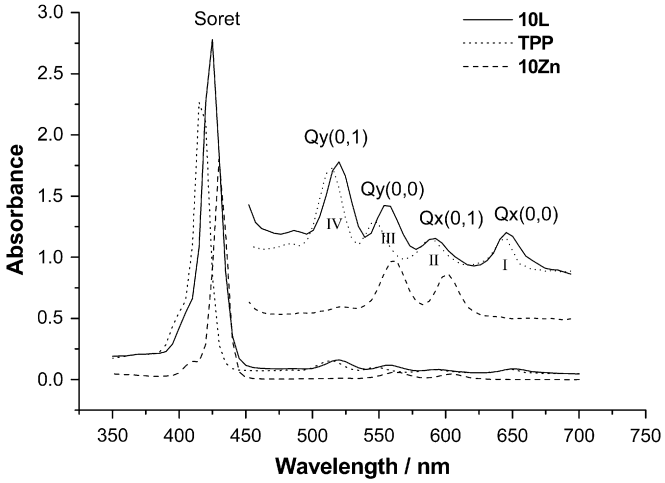

Fig. 4. Absorption spectra of TPP, **10L** and **10Zn** in DMF at room temperature.

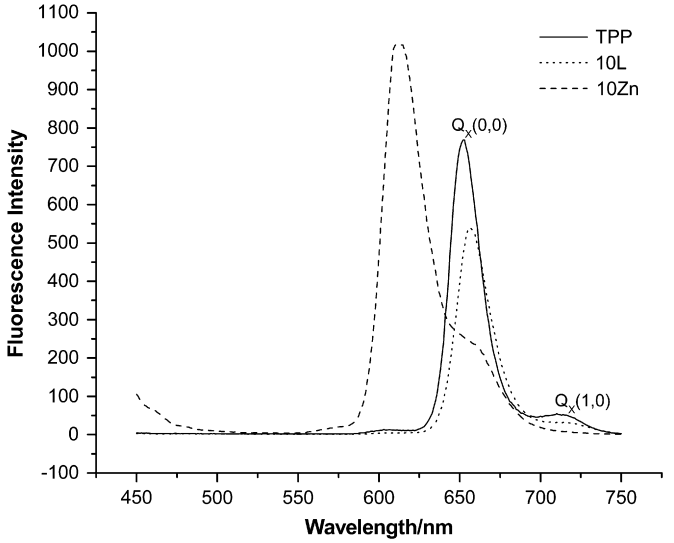

Fig. 5. Fluorescence spectra of TPP, **10L** and **10Zn** in DMF at room temperature. Fluorescence excitation wavelength $\lambda_{ex} = 420$ nm, concentrations of compounds are 1×10^{-5} mol/L.

to the red region by 2–5 nm. The fluorescent bands of Zn complexes are in the regions of 612–613 and 655–660 nm, which have shifted to the red region compared to TPPZn (604, 652 nm). This red shift may be due to the interaction of alkylamido group with the conjugated π-electron system of TPP molecules. The porphyrin macrocycle conjugation is affected by the electronic donating groups. The conjugation is enhanced when the alkylamide groups linked on the phenyl group.

The quantum yield of porphyrin ligands and Zn complexes were calculated according to the following equation:

$$\Phi_{sample} = \Phi_{TPPZn}(F_{sample}/F_{TPPZn})(A_{TPPZn}/A_{sample})$$

where F_{sample} and F_{TPPZn} are measured fluorescence integral areas (under the fluorescence spectra) of the sample and the reference TPPZn, respectively. A_{sample} and A_{TPPZn} are the absorbance of the sample and the reference. Φ_{sample} and Φ_{TPPZn} ($\Phi_{TPPZn} = 0.033$ [24]) are the quantum yields of the sample and the reference TPPZn at the same excitation wavelength. The effect of solvent is neglected. As we can see from Table 2, the quantum yields of porphyrin ligands are much lower than that of TPP. As we know, the porphyrins can be considered as a specific donor–acceptor system, and the decrease in the fluorescence quantum yields of porphyrin ligands in comparison with that of TPP can be a result of intramolecular energy migration or electron transfer from the donor part of the molecule to the acceptor part. While the fluorescence intensities and quantum yields of Zn complexes are much higher than that of the porphyrin ligands. This maybe caused by the effect of the axis coordination of the Zn complex.

Table 2
Emission spectra data of the ligands and Zn porphyrin complexes.

Compounds	Solvent	λ_{ex}(nm)	Q (0–1)	Q (0–2)	Φ
TPP	DMF	420	653	715	0.110
8L	DMF	420	655	720	0.043
10L	DMF	420	656	717	0.025
12L	DMF	420	657	720	0.023
14L	DMF	420	657	721	0.019
16L	DMF	420	657	718	0.045
18L	DMF	420	656	717	0.057
8Zn	DMF	420	613	655	0.066
10Zn	DMF	420	613	656	0.058
12Zn	DMF	420	612	659	0.071
14Zn	DMF	420	613	660	0.061
16Zn	DMF	420	612	658	0.062
18Zn	DMF	420	612	656	0.063

Table 3
Summary of redox potentials for ligands and Zn porphyrin complexes.

Compounds	E_{ox2}/V	E_{ox1}/V	E_{red1}/V	E_{red2}/V	$\Delta E^a/V$
8L	0.789	0.649	−1.490	−1.940	2.139
10L		0.626	−1.512	−1.964	2.138
12L		0.637	−1.495	−1.958	2.132
14L		0.643	−1.504	−1.955	2.147
16L			−1.510		
8Zn		0.379	−1.770		2.149
10Zn		0.450	−1.789		2.239
12Zn		0.390	−1.767		2.157
14Zn	0.672	0.359	−1.783	−2.185	2.142
16Zn		0.317	−1.801	−2.216	2.118
18Zn		0.358	−1.791		2.149
TAPP			−1.483	−1.920	
TPP			−1.270	−1.734	

[a] $\Delta E = E_{ox1} - E_{red1}$.

3.3. Electrochemistry

Cyclic voltammetric studies have been performed to evaluate the redox potentials and a summary of the redox potentials is listed in Table 3. We can see that all the ligands exhibit similar cyclic voltammograms, except **16L** and **18L** which are not soluble well in DMF. The compound of **10L** undergoes one irreversible oxidation step at $E_p = 0.626$ V which corresponds to the formation of porphyrin cation radical. There are two redox couples in the reductive scan. The first reduction potential at −1.512 V leads to the formation of porphyrin anion radical while the second at −1.964 V leads to the formation of porphyrin dianion. All Zn complexes exhibit similar cyclic voltammograms and they undergo one irreversible oxidation and one or two reversible reduction within the potential range of the solvent. The porphyrin HOMO–LUMO gap can be expressed as ΔE, the potential difference between the first oxidation and the first reduction. The experimental ΔE values of porphyrin ligands are in the range of 2.132–2.147 V, and the ΔE values of Zn complexes are in the range of 2.118–2.239 V, which are very close to the calculated values of 2.25 ± 0.15 V, obtained by

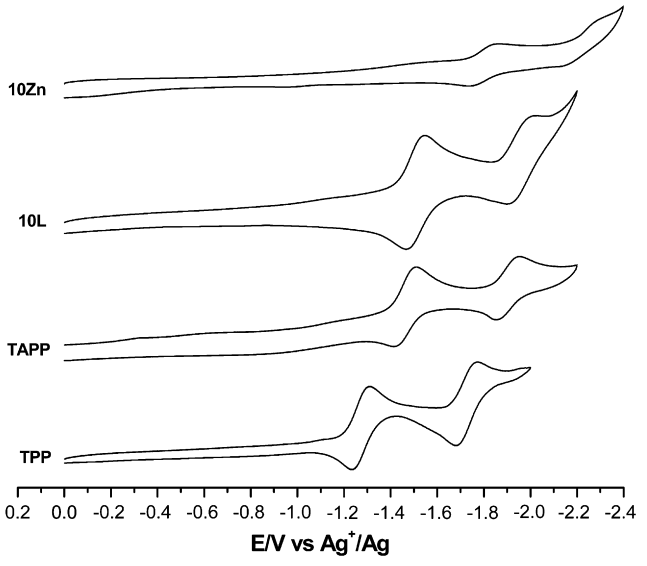

Fig. 6. Cyclic voltammograms illustrating the reductions of TPP, TAPP, **10L** and **10Zn** in DMF, scan rate = 100 mV/s.

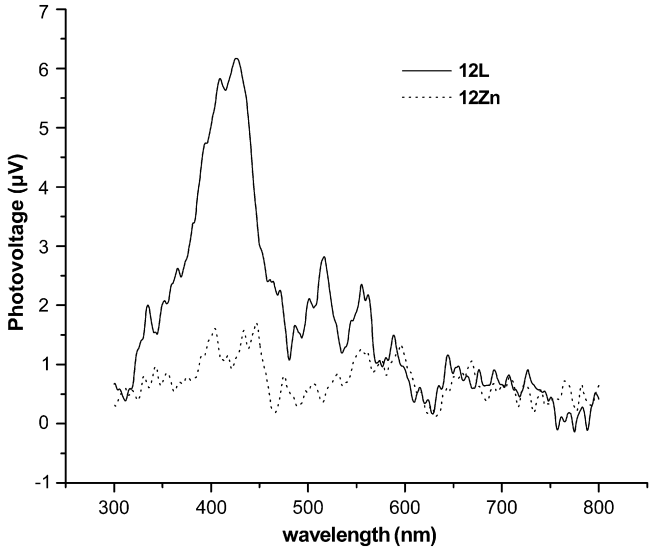

Fig. 7. SPS spectra of **12L** and **12Zn**.

Zerner and Gouterman [25]. The results show that the redox centers of the porphyrin ligands and Zn complexes are on the porphyrin ring.

Cyclic voltammograms illustrating the reductions of TPP, TAPP, **10L** and **10Zn** in DMF, containing 0.1 mol/L TBAP as supporting electrolyte are shown in Fig. 6. Comparing the data of **10L** with that of TPP and TAPP indicates that the processes are shifted toward negative potentials. The difference is 242 mV compared to TPP and 29 mV compared to TAPP for the first reduction, and 230 mV compared to TPP and 44 mV compared to TAPP for the second reduction. This can be explained by the attachment of an electron-donating group at *para* position of the four phenyl groups. The half-wave potentials would shift in a manner predicted by the Hammett linear free energy relationship $\Delta E_{1/2} = 4\sigma\rho$ [26], where σ is the total polar substituent constant which is dependent on the kind and position of the four substituents, and ρ is the reaction constant which is given in volts and expresses the susceptibility of the electrode reaction to the total polar effect of the substituents. The reduction potentials of **10L** shift only a little compared to TAPP, indicating that their σ values are very close.

From Table 3, we can see that the potentials of the Zn complexes are much negative to porphyrin ligands, which confirms that the reduction of the Zn complexes is more difficult. This can be

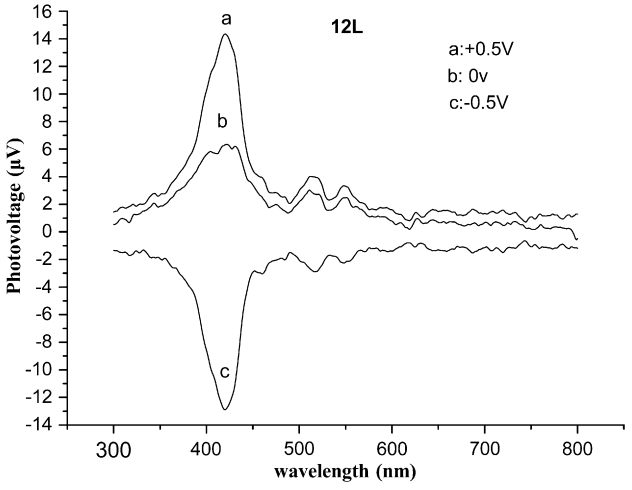

Fig. 8. EFISPS spectra of **12L** thin film under positive and negative external fields.

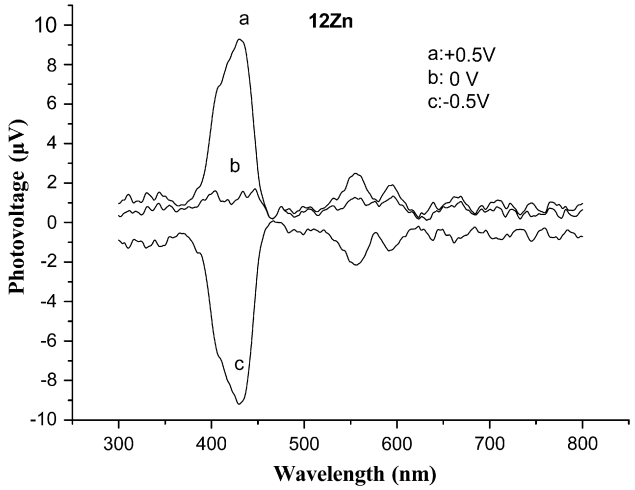

Fig. 9. EFISPS spectra of **12Zn** thin film under positive and negative external fields.

explained that the potentials of the ring centered redox sites are related to the electron density in the macrocycle. As expected, the length of the side chains has no much effect on the redox potentials, because the substituent constants of the compounds are similar.

3.4. SPS and EFISPS

The SPS and EFISPS of **12L** and **12Zn** are shown in Fig. 7. The SPS spectra in the visible region are similar to the UV–vis spectra in shape, indicating that they are corresponding to similar electron transition process. But there are also some difference between the SPS spectra and absorption spectra. First, the surface photovoltage response peaks (especially at 420 nm of **12L**) are obviously wider than the corresponding peaks in the UV–vis spectra. Second, there are only two obvious Q bands of **12L** in the SPS spectra, which are 515 and 550 nm. The number of the peaks of Q bands has been decreased. Finally, the Soret band of **12Zn** in SPS spectra is not clear; it splits to two bands, 410 and 440 nm. The difference between the SPS spectra and absorption spectra maybe caused by the status of the compounds, the UV–vis spectra show the light absorption process of a single molecule in the solution, while the surface photovoltage spectra are obtained from the photovoltage response of compound's condensed phase [27]. From Fig. 7, we can also detect that the SPS intensity of **12L** is stronger than **12Zn**, while the fluorescence intensity of **12Zn** is stronger than **12L**. This is same with Ref. [28], indicating that the fluorescence of a compound is strong, and then its photovoltage response is weak.

The surface photovoltage responses of **12L** and **12Zn** in different external electric fields are shown in Figs. 8 and 9. By comparing the spectral peaks, it is found that there is a "simultaneous response" with the change in the applied positive or negative electric field. But the intensity of those bands changes in different ways. The Soret band increases dramatically, while the Q bands change a little. A simultaneous response to the electric field indicates that all photovoltages can be assigned to $\pi \rightarrow \pi^*$ transitions. The dependence of photovoltage on the applied voltage is almost symmetric for the positive and negative fields, which confirmed that photogenerated electrons (holes) are trapped in the sample under the positive (negative) field, and left photogenerated holes create surface photovoltage.

4. Conclusion

A series of 5,10,15,20-*tetra*(4-alkylamidophenyl)porphyrin ligands and their Zn complexes have been prepared and measured

through a range of techniques, such as DSC, cyclic voltammetry, XRD, CV, fluorescence, SPS and EFISPS. Results indicate that only the ligands with long chains of more than 12 carbon atoms are mesogenic while the Zn complexes are not. Importantly the alkylamidophenylporphyrins are a new class of liquid-crystal materials. They exhibit high phase transition temperatures and broad mesophase temperature span. We studied the photophysical and electrochemical properties of the compounds, which indicated that covalent linking of alkylamido group to the tetraphenylporphyrin molecule significantly changes the structure and properties of the porphyrin macrocycle, but the length of the side chains has little effect on the properties. The results of SPS and EFISPS show that all samples are *p*-type semiconductors and the spectral bands of the compounds correspond to $\pi \rightarrow \pi^*$ transitions.

References

[1] Wasielewski MR. Chem Rev 1992;92:435–61.
[2] Gust D, Moore TA. Top Curr Chem 1991;159:103–51.
[3] Bushby RJ, Boden N, Kilner CA, Lozman OR, Lu Z, Liu Q, et al. J Mater Chem 2003;13:470–4.
[4] Gearba RI, Bondar AI, Goderis B, Bras W, Ivanov DA. Chem Mater 2005;17:2825–32.
[5] Goodby JW, Robinson PS, Teo BK. Mol Cryst Liq Cryst 1980;56:303–9.
[6] Shimizu Y, Ishikawa A, Kusabayashi S. Chem Lett 1986:1041–4.
[7] Gregg BA, Fox MA, Bard AJ. J Am Chem Soc 1989;111:3024–9.
[8] Shimizu Y, Miya M, Nagata A. Chem Lett 1991;1:25–8.
[9] Bimal RP, Kenneth SS. J Am Chem Soc 1998;120:11802–3.
[10] Liu W, Shi YH, Shi TS. Chem Res Chin Univ 2004;20:20–3.
[11] Li JZ, Xin H, Li M. Liq Cryst 2006;33:913–9.
[12] Eichhorn HJ. Porphyrins Phthalocyanines 2000;4:88–102.
[13] Ohta K, Yamaguchi N, Yamamoto I. J Mater Chem 1998;8:2637–50.
[14] Boden N, Movaghar B. Handbook of liquid crystals, vol. 2B. Weinheim: Wiley–VCH; 1998. pp. 781–98.
[15] Simmerer J, Glüsen B, Paulus W, Kettner A, Schuhmacher P, Adam D, et al. Adv Mater 1996;8:815–9.
[16] Wendorff JH, Christ T, Glüsen B, Greiner A, Kettner A, Sander R, et al. Adv Mater 1997;9:48–52.
[17] Clements J, Boden N, Gibson T, Chandler R, Hulbert J, Ruck-Keene EA. Sens Actuatators B 1998;47:37–42.
[18] Liu CY, Pan HL, Fox MA, Bard AJ. Science 1993;261:897–9.
[19] Bock H, Helfrich W. Liq Cryst 1995;18:387–99.
[20] Kruper WJ, Chamberlin TA, Kochanny M. J Org Chem 1989;54:2753–6.
[21] Nakai T, Ban K, Ohta K, Kimura M. J Mater Chem 2002;12:844–50.
[22] Paschenko VZ, Evstigneeva RP, Gorokhov VV, Luzgina VN, Tusov VB, Rubin AB. J Photochem Photobiol B 2000;54:162–7.
[23] Horrocks Jr WD, Wong CP. J Am Chem Soc 1976;98:7157–62.
[24] Quimby DJ, Longo FR. J Am Chem Soc 1975;97:5111–7.
[25] Zerner M, Gouterman M. Theor Chim Acta 1966;4:44–63.
[26] Kadish KM, Morrison MM. J Am Chem Soc 1976;98:3326–8.
[27] Shi YY, Zheng WQ, Li ZH, Wang XQ, Wang DJ, Qiu SL, et al. Opt Mater 2006;28:1178–86.
[28] Qi MH, Liu GF. J Mater Chem 2003;13:2479–84.